Journal of Materials Chemistry A

Accepted Manuscript

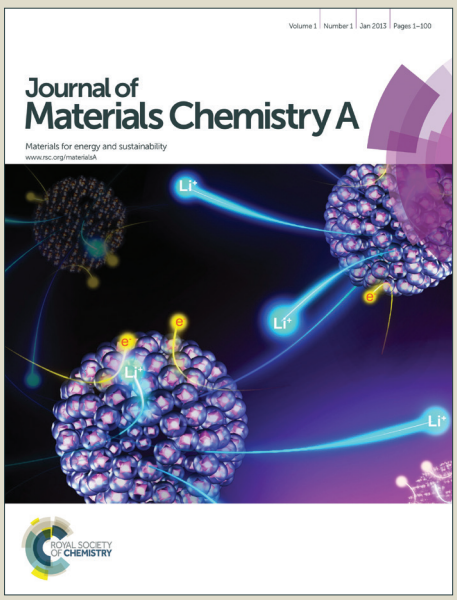

ROYAL SOCIETY OF CHEMISTRY

www.rsc.org/materialsA

New Fe_2TiO_5-based nanoheterostructured mesoporous photoanodes with improved visible light photoresponses

E. Courtin[a], G. Baldinozzi[b], M. T. Sougrati[c], L. Stievano[c], C. Sanchez[a], Ch. Laberty-Robert[a,]*

a. Laboratoire de Chimie de la Matière Condensée de Paris, UPMC−Collège de France, CNRS, Collège de France 11 Place Marcellin Berthelot, 75005 Paris

b. Matériaux fonctionnels pour l'énergie, CEA−CNRS−Ecole Centrale Paris, CEA/DEN/SRMA 91191 Gif−sur−Yvette and SPMS, 92295 Châtenay−Malabry, France

c. ICGM − UMR5253− Equipe AIME, Université Montpellier II, 2 Place Eugène Bataillon − CC 1502, 34095 Montpellier CEDEX 5

KEYWORDS. Thin Films, nanoheterostructures, mesoporous, photoelectrolysis, energy conversion

ABSTRACT

Triphasic nanocrystalline porous materials based Fe_x-TiO_2 Anatase, pseudo−brookite and Hematite are generated via a simple templated growth based strategy followed by carefully controlled temperature/atmosphere treatments. As shown by XRD, SEM, TEM experiments the resulting nano−crystaline mesoporous films exhibit optimized bicontinuous pore-solid architectures and high surface-areas. Mössbauer spectroscopy, XPS analyses indicate that Fe^{III} is the main iron oxidation state present into the films.

Moreover the materials band gaps can be adjusted between 3.3 eV and 2.18 eV by increasing the iron/titanium ratio thus allowing to tune materials absorption with the visible light electromagnetic spectrum. The nanocrystalline films prepared with a Fe/Ti ratio of 0.2 and a temperature treatment of 500°C exhibit very interesting photoelectrochemical responses. Indeed, while under visible light excitation, 500°C calcined mesoporous films made of pure nanocrystalline titania or pure nanocrystalline hematite are photocurrent silent, our triphasic nanocrystaline porous films exhibit much higher photocurrents i.e. 100 µA/cm². These interesting photoanodes are made of in situ generated nanoheterostructures built with three different nanocrystalline phases (6 nm sized TiO_2 anatase, 25 nm sized Fe_2TiO_5 pseudo-brookite that has been synthesized for the first time at low-temperature and short annealing time and 20 nm sized Fe_2O_3 hematite). As a consequence, the numerous nanoheterojunctions present in the photoanode decrease bulk electron−hole recombinations allowing an enhancement of the observed photocurrents. Furthermore, photoelectrochemical performances were optimized through the deposition of Co-based catalysts that limit surface carriers recombinations. Indeed, at 1.23 V, the optimized Co-deposited nanoheterostructured layers exhibit photocurrents higher than 0.15 mA/cm². It is worth mentioning that these photocurrents are many times higher than those observed for Co-based Fe_2O_3 nanocrystalline mesoporous layers. Moreover, the photocurrent onset potential recorded for the nanocomposite Fe_2TiO_5 peudo−brookite based photo-anodes was decreased by 100 mV. The results reported with these new nanoheterostructured mesoporous materials with large interfacial area in contact with the electrolyte shed some light on a smart concept: nanoscale controlled heterogeneity can be better than purity and homogeneity. This work opens new avenues for materials performances enhancement in solar driven water splitting.

Exploitation of abundant but intermittent and diluted renewable energy sources is one of the greatest challenges of the 21st century [1]. In particular, the production of hydrogen from solar energy through the overall splitting of water appears as a promising approach and several studies have been undertaken to reproduce the natural photosynthesis. The different strategies concern either the development of molecules and/or materials that drive both the absorption of light and electrocatalysis. The key challenges are the design of a photoelectric cell (PEC) capable of producing fuel at 10 times the efficiency of natural photosynthesis. This device will be able to harvest sunlight to generate chemical fuel by splitting water to generate hydrogen [2]. To make these systems efficient and commercially viable, the materials for the photoelectrode have to fulfill several criteria such as : (i) a small semiconductor bandgap for ample solar light absorption, (ii) conduction and valence band energies that straddle water oxidation and reduction potentials, (iii) high conversion efficiency of photogenerated carriers to the water splitting products, (iv) durability in aqueous environments and (v) low cost[3]. But, to date, no single material satisfies all of these requirements and often a combination of complementary semiconductors has to be considered [4]. Among the various semiconducting oxides, titanium dioxide (TiO_2 anatase) has been the favored semiconductor for water splitting applications since it was first used by Fujishima and Honda for water photolysis [5]. However, because of its large bandgap (3.2 eV) [6], TiO_2 absorbs only the ultraviolet part of the solar emission and often low conversion efficiency is observed. Additionally in TiO_2, a fast electron−hole recombination occurs due to an important density of trap states.

To overcome some of the limitations of TiO_2, its spectral response has to be shifted into the visible range and charge traps have to be created to keep electron and hole separated. Different strategies such as a modification of the surface with small band gap semiconductor, and/or band

gap narrowing via elemental doping have been explored leading to the enhancement of photocatalytic activity [7 8 9]. The most popular dopants for a modification of both the optical and photo-electrochemical properties of TiO_2 are transition metals such as Cr, Fe, Ni, V, Mn and Cu [9]. Among these transition metals, Fe doping seems particularly interesting as a band gap between 1.9 eV and 2.2eV has been reported for single Fe_2O_3 [3 10]. However, an optimum concentration of doping metal ions exists above which the photocatalytic activity decreases. This optimum Fe doping is usually in between 1 and 6.6 wt % (between 0.009 and 0.06 mol %) depending on the synthesis procedure and on the particle morphology [11 12 13 14 15 16 17]. Often, higher doping does conduce to the formation of heterogeneous semiconductor photo catalysts [18]. The functionality of these materials results both from the bulk properties of their various components as well as from the properties that are directly related to their interfaces properties [19 20]. Peng et *al.* reported interesting photo catalytic activities with heterostructures with an optimal molar ratio of 7:3 in Fe_2O_3/TiO_2 [21]. They related their enhancement of the photocatalytic properties to the formation of heterojunctions between Fe_2O_3 and TiO_2. These Fe_2O_3/TiO_2 composites improve the charge separation and thus restrain the recombination of photo generated carriers, *i.e.* electrons and holes [20]. Zhang et *al.* also observed that Fe_2O_3/TiO_2 heterostructures with high Fe contents (24 wt %) deposited by chemical vapor deposition on activated carbon fibers allowed interesting photo catalytic activities for the degradation of methyl orange [22]. Another strategy is to synthesize TiO_2 protected with Fe_2O_3 or Fe_2O_3 protected with TiO_2. [23 24 25] These results highlight the needs of improving the morphology and the electronic structure of TiO_2 to tune separation and transportation of photo−excited charge carriers. Most of the results known in photocatalysis might be transposed to water splitting application. To our knowledge, transition metal –TiO_2 photoelectrode have been scarcely studied as photoanodes. For this type of application, beside

the composition of the electrode, its nanostructuration appears to be a relevant approach to tune both the charge separation and the transportation of photo−excited charge carriers [26]. Higher efficiencies have been obtained for nanostructured photoelectrodes that exhibit nanoparticle organized in a 3−D porous network. This nanoarchitecture ensures a very short hole collection length compared with traditional photo electrodes where the light penetration depths of hundreds of nanometers is necessary [26 27 28]. This strategy was first reported by Grätzel et *al.* who synthesized a mesoporous electrode composed of hematite particles with size between 25 and 75 nm[29]. Several additional methods to fabricate a variety of photo electrodes nanostructures, including nanoparticles [30], nanowires [30 31], nanotubes [32], nanocauliflowers [33] have also been reported. Mesoporous transition metal−oxide films appear to be an interesting approach leading to an improvement of the photocurrent [34 35 36]. This is related to the thin walls of the mesopores, which provide a short distance for the excited electrons and holes to travel to the surface, limitating the electron−hole recombination. However, most of these mesoporous structures are synthesized via specific and/or costly instruments such as atomizers, chemical vapor deposition or spray pyrolysis systems and use toxic precursors and/or solvents [3 33]. Owing to these aspects, the development of facile, cost−effective and environment friendly method, such as sol−gel synthesis coupled with the dip−coating technique constitutes an interesting approach to synthesize mesoporous thin films [36 37]. Compared to other chemical approaches [20 33], the sol−gel process allows a very good control of the film microstructure through a careful tuning of the sol composition, the heat treatment and the deposition conditions [38 37]. But, while the nanostructuring of the photoelectrode limits the e^-/h^+ recombination occurring in the bulk, surface hole recombination might occur due to the slow oxygen evolution reaction (OER) kinetics at the surface of the photo anodes. This effect has been mostly observed and studied at

the surface of hematite. As a consequence, a large potential has to be applied to drive water oxidation reaction [39 40]. To overcome these limitations, the addition of Ir or Ru−based catalysts at the surface of the photo anodes [41], as well as nickel oxide or cobalt-based catalysts, which are more abundant and less expensive, have been explored and a reduction of the photocurrent onset potential is usually observed [42 33]. Electrodeposition as well as dip−coating or wet impregnation are usually used to deposit these electro−catalyst [33 43 44].

In this study, we report a simple method to produce mesoporous Fe−TiO_2 films (with x representing the Fe content in percent) that have a suitable vanlence band structure to photo−oxidize water to O_2 while having a band gap covering the entire range of visible light. Fe−TiO_2 films exhibit hetero−structure depending on the Fe content that limitates the e^-/h^+ recombination. TiO_2 compounds containing Fe^{3+} were reported to have a band gap of ~2.3 eV and exhibit p-n junction[45]. Owing to this feature, TiO_2 containing Fe^{3+} ions having bandgap energy of ~2.3 eV have been reported as photo−catalysts. However, to the best of our knowledge, none of these Fe_x− TiO_2 mesoporous films have been investigated for solar energy conversion to date. This study for the first time highlights a sol−gel chemistry route coupled with template to synthesize new nano-heterostructured mesoporous materials with large interfacial area as photoanodes for solar hydrogen production.

Method and Materials.

Chemicals. $Fe(NO_3)_3$, 9 H_2O, (≥ 98 %), $TiCl_4$ (99.9 %), $Co(NO_3)_2$, 6 H_2O (≥ 98 %) and anhydrous ethanol were purchased at Sigma−Aldrich. Poly−iso−butylene−polyethyleneoxyde (PIB−*b*−PEO: P4973−IbEO, M.W. (PIB) = 7000 $g.mol^{-1}$ and M.W. (PEO) = 8500 $g.mol^{-1}$) was purchased at Polymer Source. All chemical reagents were obtained from commercial sources as

guaranteed−grade reagents and used without further purification. Fluorine−doped Tin Oxide (FTO) – coated substrates (YSUB/ASASHI120/1: 10 x 30 mm) were purchased at SOLEMS (Resistivity: 80 Ω, thickness of FTO layer : 80 nm).

Solutions. First, a solution containing the $TiCl_4$ precursor was prepared by mixing $TiCl_4$ and Ethanol (EtOH). The following solution composition was chosen: $TiCl_4$: EtOH with a molar ratio of 1 : 5. $Fe(NO_3)_3$, 9 H_2O was added into this solution following the molar ratios : Ti : Fe = 1 : 0 (TiO_2), Ti : Fe = 0.99 : 0.01 ($Fe_{0.01}$−TiO_2), Fe : Ti = 0.9 : 0.1 ($Fe_{0.1}$−TiO_2), Fe : Ti = 0.8 : 0.2 ($Fe_{0.2}$−TiO_2) and Ti : Fe = 0.7 : 0.3 ($Fe_{0.3}$−TiO_2). Secondly, 100 mg of PIB−*b*−PEO was dissolved in a mixture of 5.0 g EtOH and 0.4 g H_2O by heating at 70°C for 1 hour. After cooling, the solution of PIB−*b*−PEO was added dropwise in the inorganic sol. The concentration of inorganic salts in the final solution was 0.5 $mol.L^{-1}$. The Fe_x−TiO_2 mesoporous films were synthesized by a template−directed sol−gel synthesis coupled with the dip−coating process onto glass substrates [37 46]. A FTO (Fluorine-doped Tin oxide)−layer onto glass substrate is dip−coated into the solution and then removed with a speed of 2.5 $mm.s^{-1}$ in dry atmosphere resulting in an initial hybrid, transparent and homogeneous film. The films were then placed for 60 min in a furnace pre−heated at 500°C in air (static atmosphere) to induce crystallization and decompose the block−copolymer. For tuning the thickness and the properties of the films, a multi−layers synthesis was undertaken. Multi−layered films were obtained by performing several (one to five) cycles of dip−coating and thermal treatment at 430 °C for 5 min to stabilize the layer, before a final thermal treatment at 500°C for 15 min in air. The thickness of the films was evaluated from cross−section FE−SEM images. A film thickness of ~500 nm was obtained for 5 deposited layers. For tuning the defects concentration and thus the electrical properties of the films, heat−treatment under reducing atmosphere has been performed. Mesoporous Fe−TiO_2 films

calcined at 500°C for 15 min were heated in 5% H_2/Ar atmosphere for 30 min at two temperatures: 200°C, 300°C.

Film sensitization by Co−based catalyst. The Co−based catalyst was deposited onto mesoporous $Fe_{0.2}$−TiO_2 thin film by impregnation approach [37]. The mesoporous $Fe_{0.2}$−TiO_2 thin film was dipped in an aqueous solution of $Co(NO_3)_2$, 6 H_2O (10 mmol.L^{-1}) for 1 hour. The "Co-based electrocatalyst" deposited onto $Fe_{0.2}$−TiO_2 film was then washed with deionized water and dried at room temperature prior to photo electrochemical measurements. The quantity of Co−based electrocatalyst deposited at the surface of the electrode was estimated by SX−Five CAMECA microprobe.

Characterization. The structure of the mesoporous thin films was measured using a Bruker AXS D8 Discover X-ray diffractometer. The measurements in glancing geometry were performed using a line focus Copper X-ray tube and a parabolic multilayer Göbel mirror to obtain an almost parallel x-ray CuKα impinging beam. A primary slit of 0.1mm x 6 mm was used to obtain a square footprint on the sample for a 1° glancing angle. The samples were mounted on a motorized X, Y, Z stage, supported by an Eulerian cradle, to obtain an accurate alignment of the samples at the goniometer center. The penetration depth of the X-ray beam for a 1° glancing angle is about 245 nm for the Fe_2TiO_5 compound. The penetration depth is a function of the Fe composition, but such a glancing angle always allows the selective probing of the mesoporous layers, keeping, at the same time, a limited instrumental contribution to the peak broadening [47]. This choice allows determining with great accuracy the size of the nanocrystals and the eventual microstrain in the mesoporous samples [48]. A 1D position sensitive detector LynxEye (2° angular opening) was used to speed up the data collection. A parasitic fluorescence signal is always observed in samples with significant concentrations of Fe atoms shined with

copper radiation: therefore, prior to these measurements, the energy discrimination of the detector was optimized to get the best peak to background ratio. The measured diffraction patterns ($3.5°<2\theta<140°$, $\Delta 2\theta=0.02°$, $\alpha=1°$) were refined using the Rietveld software XND[49].

The elemental composition of the film was determined by ICP (Inductively Coupled Plasma)-OES (Optical Emission Spectroscopy).

The microstructure of the films obtained after different heat treatments was observed by Field Emission (FE) Gun Scanning Electron Microscopy (FE−SEM, Hitachi) and by High Resolution Transmission Electron Microscopy (HRTEM) using a JEOL JEM 2010 instrument equipped with a field emission gun operated at 200 kV. For HR−TEM analyses, the films were scratched from the FTO substrates and the obtained powders were deposited onto carbon coated–copper grids.

^{57}Fe Conversion Electron Mössbauer spectra (CEMS) were measured with a source of ^{57}Co in rhodium metal. During the measurements, both the source and the absorber were kept at ambient temperature (294 K). The spectrometer was operated with a triangular velocity waveform. The velocity scale was calibrated with the magnetically split sextet spectrum of a high−purity α−Fe reference absorber. The samples were mounted in a gas−flow proportional CEMS detector, and a He gas−flow was used to enhance the electron signal. The spectra of the measured samples were fitted to appropriate combination of Lorentzian profiles representing hyperfine magnetic sextets and quadrupole doublets by least−squares methods using the program PC-Mos II. In this way, spectral parameters such as the hyperfine magnetic field (B), quadrupole splitting/shift (Δ/ε), isomer shift (δ) and relative resonance areas of the different spectral components were determined. Isomer shifts are given relative to α-Fe metal.

X−Ray Photoelectron Spectroscopy (XPS) was performed with a Perkin−Elmer spectrometer operating at 350 X using standard Al radiation. The pressure was below 5 x 10^{-8} Pa. The spectrometer was calibrated by assuming the binding energy of the Au4f7/2 line to be 83.4 eV relative to the Fermi level. The reported BEs were corrected to account for the charging effects by assigning the BE value of 284.6 eV to the C1s line of carbon.

UV−Visible absorption spectra were measured on an Agilent Technologies Cary Series spectrophotometer.

A SX−Five CAMECA microprobe, equipped with a LaB6 source, WDS spectrometers and a Brüker EDS spectrometer was used for evaluating the quantity of Co deposited at the surface of the mesoporous films.

Electrochemical measurements were performed in a home−made cell with a Solartron Analytical Modulab potentiostat. A three electrodes configuration was used with a platinum (Pt) wire as counter electrode and an Ag/AgCl/KCl electrode as the reference electrode. The measured potentials *vs* Ag/AgCl were converted to the reversible hydrogen electrode (RHE) scale according to the Nernst equation: $E_{RHE} = E_{Ag/AgCl} + 0.059\ pH + E^{\circ}_{Ag/AgCl}$ where E_{RHE} is the converted potential *vs* RHE, $E°_{Ag/AgCl} = 0.197$ V at 25°C and $E°_{Ag/AgCl}$ is the experimentally measured potential against the Ag/AgCl reference. The Fe_x−TiO_2-coated FTO/glass samples were connected to a brass wire (Filotex) and used as the working electrode. Measurements were done in the dark and under illumination with a Xenon lamp (Oriel, ozone free) operating at 280 W, coupled with a water−filled Spectra−Physics 6123 NS liquid filter to eliminate Infra-Red radiations and a spectra−Physics 59472 UV cut−off filter (λ > 400 nm). All measurements were performed with illumination of the film/electrolyte interface through a 1 cm²

mask in the visible range only, at a distance of 40 cm from the lamp. Current−voltage (20 mV/s scan rate) measurements were performed in 1M NaOH (pH = 13.9) and 1 M NaOH with 0.5M H_2O_2 in deionized water.

For O_2 detection, a GC-2014 Shimadzu chromatograph was used with nitrogen as gas vector. 500 µL of a mixture of (N_2 and O_2) were injected and analyzed during 5 minutes at 50°C. For O_2 detection, the electrochemical cell used was gas tight and no mixture between gas formed at the working electrode and the counter electrode was possible.

Results and discussion.

The Fe_x−TiO_2 mesoporous films were synthesized by a template−directed sol−gel synthesis coupled with the dip−coating process onto glass substrates [37]. The color of the synthesized mesoporous Fe_x−TiO_2 films evolves with increasing the iron content (x): the films turn yellowish when x increases and it is then reddish for $Fe_{0.3}$−TiO_2 (Fig. 1.a.). However, at this stage X−ray diffraction analyses indicated that the initial dip-coated films were still amorphous (not shown). Thermal processing is then required to crystallize the inorganic walls and to decompose the block−co−polymer, leading to the formation of crystalline nanostructured films with an open porous network (Fig. 1). Elemental analyses were performed to evaluate the Fe/Ti ratio. In all cases, a difference between the experimental and theoretical ratio were found. This is explained by the concentration of the $TiCl_4$ solution in ethanol that was lower that the one expected due to the high reactivity of $TiCl_4$. For example, for the target x = 0.3, the experimental value for x = 0.5. The value reported in the article is then the theoretical one.

The Fe_x−TiO_2 hybrid organic−inorganic films were heated in air at 500°C for 15 min. Top−down (Fig.1b) Field Emission Scanning Electron Microscopy (FE−SEM) images show that after the

heating step the films were highly porous and uniform. Thermal treatment at a higher temperature (up to 600°C) in air does not change the films microstructure of the films but it does decrease the conductivity of the FTO substrate (Fig. S1). Accordingly, the final heat−treatment of the film is thus fixed at 500°C in air for 15 min. The microstructure of the film evolves with the iron content as indicated Fig. 1.b. For high Fe content, the films have a worm−like open mesostructure instead of well−defined pores as those observed for pure mesoporous TiO_2. This change in mesostructure is related to phases segregation and grain growth in the pore walls, as shown by X−ray diffraction analyses (Figs.1. c). The cristallinity and the structure of the films were then studied through ex−situ X−ray diffraction analyses and the results as function of the iron contents are reported in Fig. 1.c. The film doped with the lowest amount of Fe (1 %) exhibits peaks that correspond only to the anatase structure (ICCD 00−001−0562). But, for $Fe_{0.1}$−TiO_2 films, peaks corresponding to pseudobrookite (Fe_2TiO_5: ICCD 00−041−1432) and anatase are observed. For $Fe_{0.2}$−TiO_2, three phases co−exist in the structure: a majority of pseudobrookite, some anatase and traces of hematite (ICCD 04−003−2900), whereas, for the highest Fe concentration ($Fe_{0.3}$−TiO_2), pseudo−brookite is only observed with traces of hematite. The average crystallite size for the different phases observed in the films was determined using Rietveld refinement (Table S.1). Addition of Fe limits the crystal growth as TiO_2 anatase grains as an average crystallite size as small as 6 ± 1 nm is observed for the $Fe_{0.2}$−TiO_2 film. In parallel, the grain size of the pseudobrookite increases from 12 to 25 nm with the Fe content. These observations are confirmed by HR−TEM analyses that indicated the presence of nanocrystallites (Fig. 1.d). Lattice fringes are visible, reflecting the cristallinity of the Fe_x−TiO_2. Indeed, crystallized grains with a wide distribution of sizes are observed for the composition $Fe_{0.3}$−TiO_2. The smallest grains (~ 15 nm) show an interplanar spacing of approximately 0.36 nm,

corresponding to hematite (Fe_2O_3: ICCD 04−003−2900) while bigger grains (~ 25 nm) correspond to crystallized pseudobrookite (Fe_2TiO_5: ICCD 00−041−1432) with an interplanar distance of 0.49 nm. HR−TEM images for samples $Fe_{0.01}$-TiO_2 and $Fe_{0.1}$−TiO_2 was also performed and the results are reported in Figure S1 (Supporting Information). For the $Fe_{0.1}$−TiO_2 sample, grains of approximately 7 nm with an interplanar distance d = 0.35 nm, corresponding to anatase (ICCD 00−001−0562), and bigger grains of pseudobrookite with a size of ~ 20 nm are observed. For the lowest concentration of Fe ($Fe_{0.01}$−doped TiO_2), only grains of approximately 17 nm corresponding to anatase are observed.

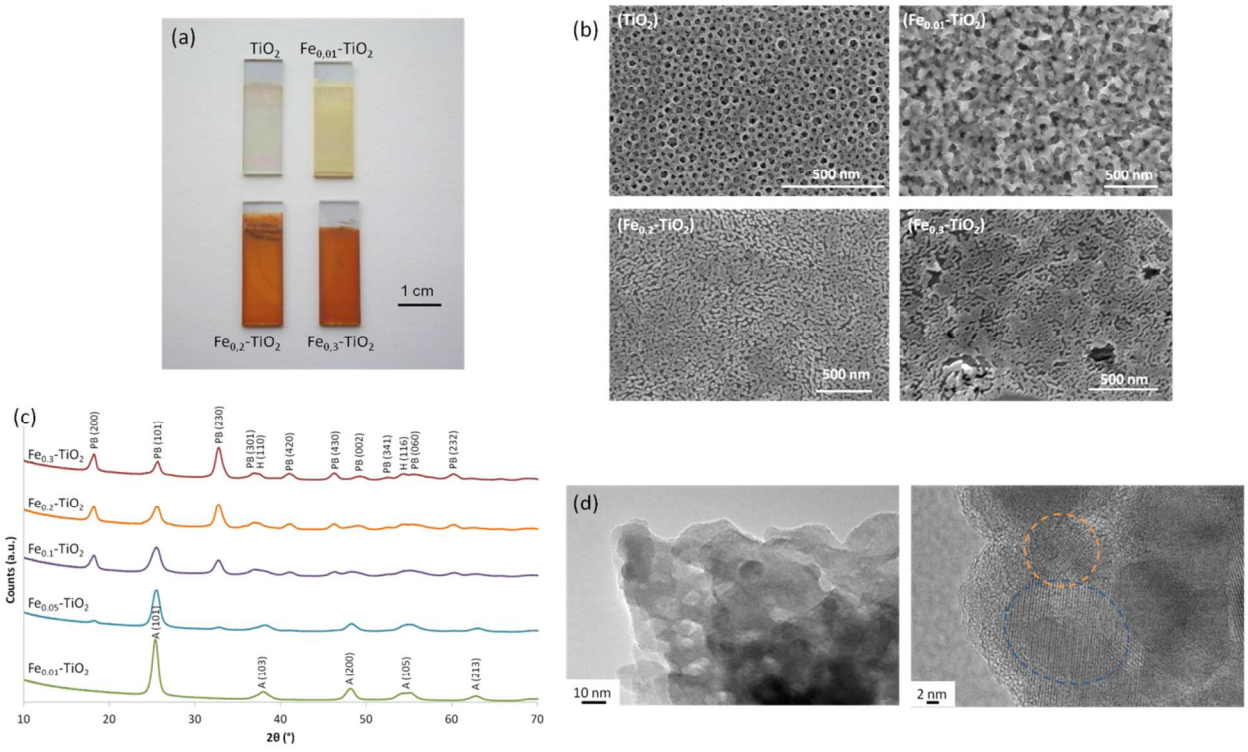

Figures 1. Structure and Microstructure of Fe_x−TiO_2 mesoporous thin films. a. Digital pictures of Fe_x−TiO_2 mesoporous films heat−treated at 500°C under air for 15 min, b. SEM images of Fe_x−TiO_2 mesoporous films heat−treated at 500°C under air for 15 min, c. XRD spectra of Fe_x−TiO_2 and d. HR−TEM of $Fe_{0.3}$− TiO_2 heat−treated at 500°C under air for 15 min.

The nature of the iron in the various components of Fe_x−TiO_2 mesoporous thin films was studied by ^{57}Fe Conversion Electron Mössbauer spectroscopy (CEMS) and XPS analyses. ^{57}Fe CEMS

provides insight on the oxidation state of the iron as well as on its local coordination environment on a surface layer of the sample about 100 nm thick. All the measured spectra exhibit a single dominant quadrupole doublet centered at about 0.35 mm/s with hyperfine parameters in the typical range of Fe^{3+} (Figure 2.a and Table S.2). The total resonance area of the Mössbauer spectra decreases from $Fe_{0.3}$-TiO_2 to $Fe_{0.1}$-TiO_2, to $Fe_{0.01}$-TiO_2, in line with the gradual decreasing of the iron loading in the samples. For the $Fe_{0.01}$−TiO_2 mesoporous film, the intensity of the spectrum is very small, and only the quadrupole doublet of Fe^{3+} is visible with a very small signal−to−noise ratio, making very difficult a precise determination of the hyperfine parameters. For $Fe_{0.1}$−TiO_2 and $Fe_{0.3}$−TiO_2, the signal−to−noise ratio is much larger, and allows one to detect, in addition to the dominant Fe^{3+} quadrupole doublet, an additional magnetic sextet with the typical hyperfine parameters of hematite (see Table S.2). The Fe^{3+} quadrupole doublet has a relatively large line width and can be fitted to two Fe(III) spectral components. The hyperfine parameters of these two components correspond well to those commonly observed for pseudobrookite, Fe_2TiO_5. Moreover, their similar intensity confirms the presence of Fe^{3+} evenly distributed in the two 8f and 4c sites of the orthorhombic crystal structure of pseudobrookite [50]. These experiments confirm that, for $x \geq 0.1$, the Fe_x−TiO_2 mesoporous films are composed of a mixture of phases including Fe_2TiO_5, Fe_2O_3 and Fe−doped anatase.

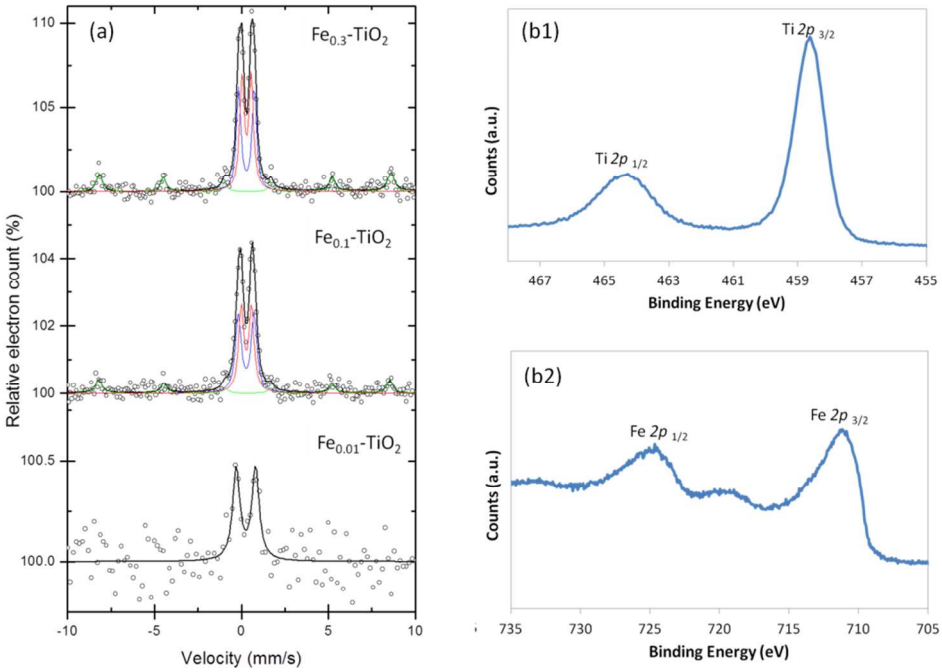

Figure. 2. Oxidation state of iron in Fe_x-TiO_2 thin films. a. Room temperature ^{57}Fe Conversion Electron Mössbauer spectra of the studied samples. From top to bottom: $Fe_{0.3}$−TiO_2, $Fe_{0.1}$−TiO_2 and $Fe_{0.01}$−TiO_2. b. XPS spectra of Ti 2p (b1) and Fe 2p (b2) of $Fe_{0.3}$-TiO_2 annealed at 500°C under air.

In agreement with CEMS, XPS also confirms that the oxidation state of iron is mainly +3 for all the studied films (Fig. 2 b). However, minor amounts of Fe^{2+} are also detected whatever the composition. The presence of small amounts of Fe^{2+} in these mesoporous films is likely related to the reduction of Fe^{3+} into Fe^{2+} at the surface of the films under the high vacuum conditions of XPS chamber [51].

The optical properties of mesoporous Fe_x−TiO_2 were studied by UV−Vis absorption spectroscopy. The light absorption edges undergo a red shift into the visible range when the Fe content increases in the mesoporous Fe_x−TiO_2 films. The band gap (Eg) was estimated from these UV spectra by using the following equation: $\alpha k \upsilon = \text{constant}(h\nu - E_g)^n$ with k: the Boltzmann constant [52 53] . By plotting $(\alpha k\upsilon)^{1/n}$ *vs*. hν, the intercept of the tangent to the absorption edge with

the abscise gives an estimation of the band gap energy, which is indirect allowed in this case (n = 2) [54 55] (Fig. S2). The estimated bandgap is 3.3 eV for TiO_2 which is close to the theoretical values (3.2 eV) [6 55] and at 2.2 eV for the $Fe_{0.3}$−TiO_2 film which is in agreement with the reported value of 2.18 eV of bulk Fe_2TiO_5 [56]. The decrease of the band−gap for Fe−substituted TiO_2 films is attributed to the formation of a dopant energy level within the TiO_2 band gap after Fe−doping. The Fe^{3+} impurity level is close in energy to the valence band of TiO_2, so electron would rather transfer from the Fe^{3+} impurity level than from the valence band to conduction band due to the lower excitation level. Additionally, the d−d transition $^2T_{2g} \rightarrow {}^2A_{2g}, {}^1T_{2g}$ of Fe^{3+} or the charge transfer transition between iron ions ($Fe^{3+} + Fe^{3+} \rightarrow Fe^{6+} + Fe^{'+}$) contribute to the enhanced absorption in the visible region [57].

The photo−electrochemical performances

To further characterize these mesoporous Fe−TiO_2 films, their electro− and photo−electrochemical properties were evaluated. First, cyclo− voltammetry (*J*−*V*) curves were measured under illumination of visible light (wavelength ≥ 420 nm) in the potential ranges 0.8 V to 2 V *vs.* RHE for various Fe contents (Figure 3, Figure S3) at pH = 13.9. Clearly, the *CV* behavior depends on the iron content. For Fe content ≥ 0.1, the electrode exhibits the typical response of hematite sample with higher photocurrent. Water oxidation photocurrent onsets is observed at + 1.03 V *vs*. RHE in NaOH electrolyte (pH = 13.9). Then, the current density increases rapidly, attaining approximately 0.15 mA/cm^2 at 1.23 V *vs.* RHE. A plateau corresponding to a current of 0.2 mA/cm^2 is obtained from 1.4 to 1.6 V vs. RHE. For Fe content > 0.2, the onset of the photocurrent shifted cathodically to + 0.8 V *vs.* RHE while the current density decreases and reaches a value of 0.05 mA/cm^2 at 1.23 V and 0.1 mA/cm^2 at 1.43 V *vs*.

RHE. These values are clearly superior to those of the control sample, α−Fe_2O_3 synthesized in the same conditions, over the full bias range[37].

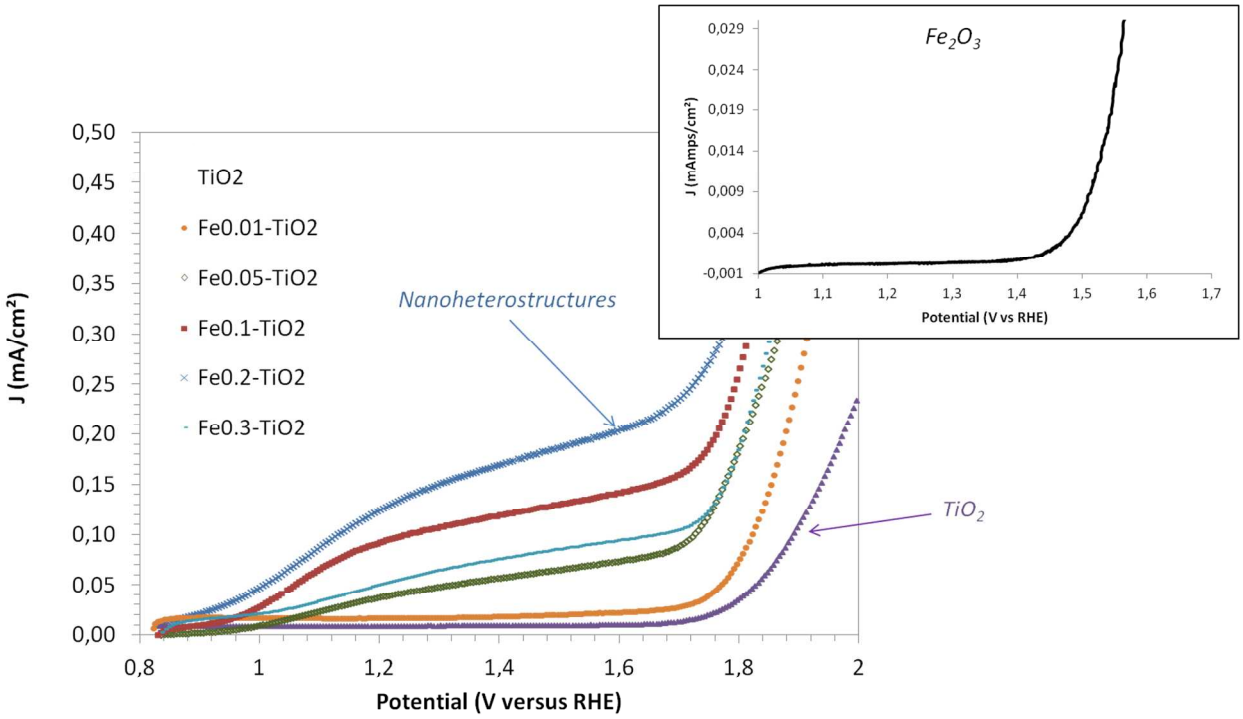

Figure 3. Current density *vs* applied potential (J−V) plots for the Fe−TiO_2 electrodes as function of Fe content under visible light illumination. Inset is the Fe_2O_3 plot measured in the same conditions. The curves were measured in 1 M NaOH aqueous solution (pH = 13.9).

Figure. 4a. shows the water oxidation photocurrent density attained at 1.23 V *vs.* RHE as a function of the iron content. The photocurrent increases with the quantity of iron up to x = 0.2. A further increase in the Fe content does not lead to further improvement. On the contrary, the photocurrent decreases. This result indicates that the best photo−current is achieved for Fe_x−TiO_2 with x = 0.2. These films contain three different nanocomponents; Fe-doped anatase, pseudo−brookite, and traces of hematite. The enhancement of performance observed might be explained by the presence of multiple nanoheterojunctions in the film with differing electron

affinities that can suppress detrimental charge recombination[19]. Indeed, we observe that the maximum current density was obtained for a much higher Fe concentration than for Fe−containing films usually described in the literature (~ 1 wt. %)[11, 14, 16]. The resulting gas obtained after 6 hours of splitting with the $Fe_{0.2}$-TiO_2 film under illumination at 1.5 V vs RHE were analyzed by Gas Chromatography (Figure S4). The chromatogram shows one peak at 1.37 minutes, which can be only attributed to Oxygen by comparison with the Oxygen contained in air (extraction time: 1.37 minutes). This demonstrates that the photo-current passing through the photo-anode results in oxygen production.

Photocurrent transient measurements were performed in order to assess the dynamic of water oxidation and charge recombination at the mesoporous film/electrolyte interface. To summarize, the potentials are changed from 0.8 V to 1.5 V *vs.* RHE while illumination is turned on and off and the time−resolved photocurrent is recorded.

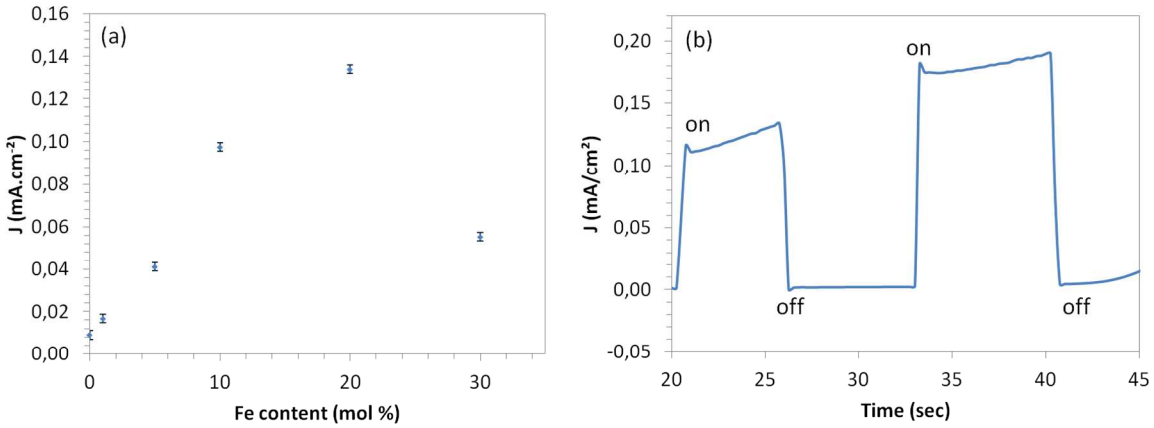

Figure 4. (a) Current density of the electrodes as a function of Fe content at 1.23 V *vs* RHE. (b) Chopped light photocurrent response of the $Fe_{0,2}$-TiO_2 thin film electrode. The curves were measured in 1 M NaOH aqueous solution (pH = 13.9).

The current density is shown with respect to time in Figure 4b and Figure S5. Previous studies of photoanode transient currents indicate that when light reaches the sample, the photogenerated holes travel to the semiconductor liquid junction (SCLJ) and accumulate because of the slow oxygen electrode reaction kinetics, or because carriers oxidize trap states in the bulk and on the surface [58]. This induces a sharp anodic current spike that decreases as the accumulation process perturbs the charge distribution of the space charge region and stabilizes when equilibrium is eventually reached between water oxidation and charge recombination. Conversely, the cathodic transient peak observed when the light is turned off is assigned to electrons diffusing from the external circuit and recombining with the accumulated holes at the SCLJ. On the photocurrent curve, the presence of transient currents depends strongly on the x content. The appearance of transients is less important for x = 0.2 compared to the other mesoporous films. This clearly indicates that the mesoporous films containing the highest concentration of nanoheterostructure are more efficient because fewer holes accumulate at the SCLJ.

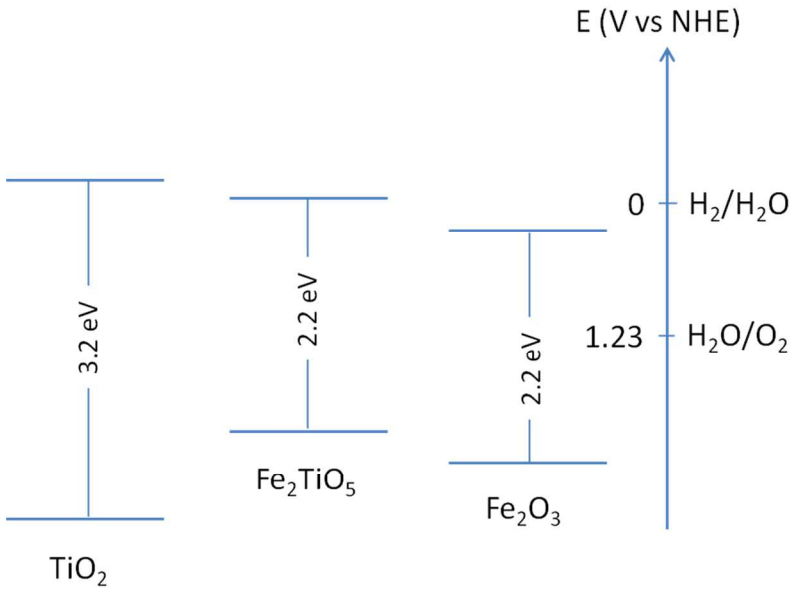

Figure 5. Position of valence and conduction band edges for TiO_2, Fe_2TiO_5 and Fe_2O_3 heterojunctions from [18]

Figure 5 shows the band diagrams of the heterojunctions based upon existing published data[18]. Fe_2TiO_5 heterojunctions would form intermediate conduction levels between TiO_2 and Fe_2O_3. In the case of $Fe_{0.2}$-TiO_2 films, where Fe_2TiO_5 is the majoritary phase, contact between Fe_2TiO_5 and Fe_2O_3 would facilitate electron transfer from the doped phase to hematite while a bias would have to be applied to allow electron transfer from Fe_2TiO_5 to TiO_2 thus limiting the photocurrant obtained from TiO_2 in the UV range. In this configuration, contact between Fe_2TiO_5 and TiO_2 or Fe_2O_3 would also facilitate hole transfert from Fe_2TiO_5 to the undoped phases and thus limit hole accumulation.

To confirm these results, an oxidized hole scavenger was used to quantify bulk and surface recombination [40]. A comparison of the photocurrent between an electrolyte solution with a hole scavenger that suppresses surface recombination with a water−based electrolyte and without hole scavenger has been performed to quantify the surface recombination. H_2O_2 has been chosen as hole scavenger because i) its transparent to visible light and UV, ii) it does not corrode $Fe_{0.2}$−TiO_2 films, iii) it has a rate constant for oxidation 10 to 100 times higher than that of water and iv) it has a relatively negative reduction potential. Current density *vs.* applied potential (*J*−*V*) plots is reported in Figure 6 for $Fe_{0.2}$−TiO_2 films and in Figure S6 for $Fe_{0.1}$-TiO_2 films in 1 M NaOH or 1 M NaOH (1 M) and H_2O_2 (0.5 M).

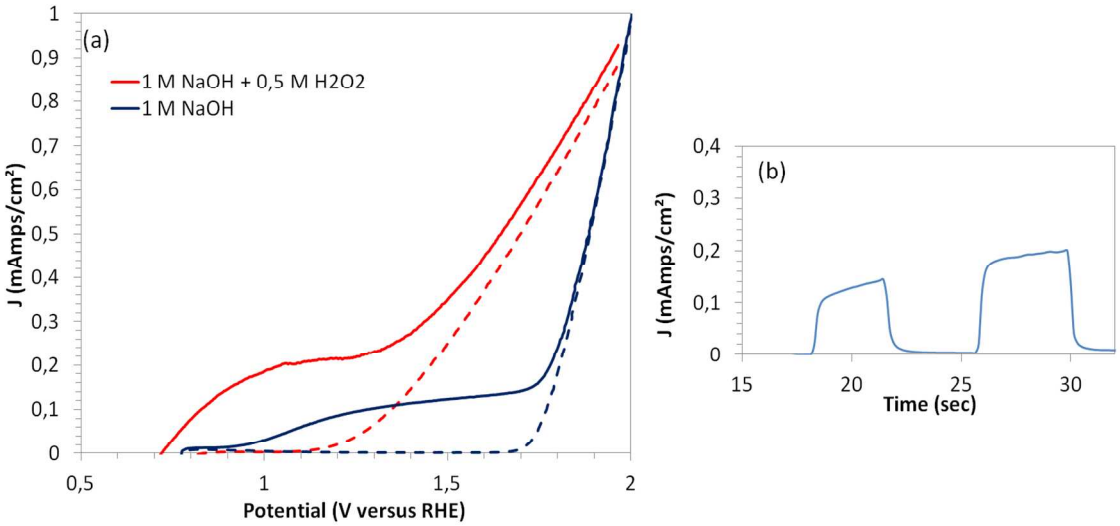

Figure 6. Suppression of the surface recombination by adding a hole scavenger into the electrolyte. a. Current density *vs.* applied potential ($J-V$) plots in dark (dotted line) and under visible light illumination of mesoporous $Fe_{0.2}-TiO_2$ thin film in either 1 M NaOH (blue) and 1 M NaOH−0.5 H_2O_2 (red). b. Chopped light photocurrent response of mesoporous $Fe_{0.2}-TiO_2$ thin film in 1 M NaOH−0.5 H_2O_2. Each light on/light off period was 10 s.

An increase of the photocurrent is observed in the whole potential range and an increase of the photocurrent, indicating that the injection barrier for minority carriers has been removed. Chopped light chronoamperometry measurements were used to examine the transient current response of the $Fe_{0.2}-TiO_2$ films under these conditions (NaOH (1M) − H_2O_2 (0.5 M)). The current transients disappeared and purely faradaic photocurrents were observed in the whole potential range, confirming that the holes arriving at the electrode/electrolyte interface contribute to the water oxidation reaction and that no recombination takes place between electrodes and photo−oxidized surface species. These results confirm that adding H_2O_2 into the electrolyte does definitively suppress surface recombination.

To overcome problems associated with surface states, we modified the surface chemistry of the mesoporous films by depositing a cobalt−based catalyst. First, the quantity of the cobalt−electro−catalyst deposited onto the surface of $Fe_{0.2}-TiO_2$ mesoporous film was estimated by SX−Five CAMECA microprobe. From this measurement, 0.2 wt. % of Co was effectively deposited at the surface of the $Fe_{0.2}-TiO_2$ mesoporous film. Then, UV−Visible spectroscopy was

performed on the thin film photoelectrode after addition of the catalyst to verify that the light absorption properties of the film were preserved (Figure S7). The current density *vs.* applied potential plots (*J*−*V*) in Figure 7 show a slight decrease in the overpotential and a slight increase in the photo−current (0.13 mA/cm^2 for the electrode without Co−catalyst and 0.17 mA/cm^2 for the electrode with the Co−catalyst) at more positive potentials. These results are related to the reduction of the hole recombination and a better water oxidation kinetics obtained through the use of "Co−based electro−catalyst" [59].

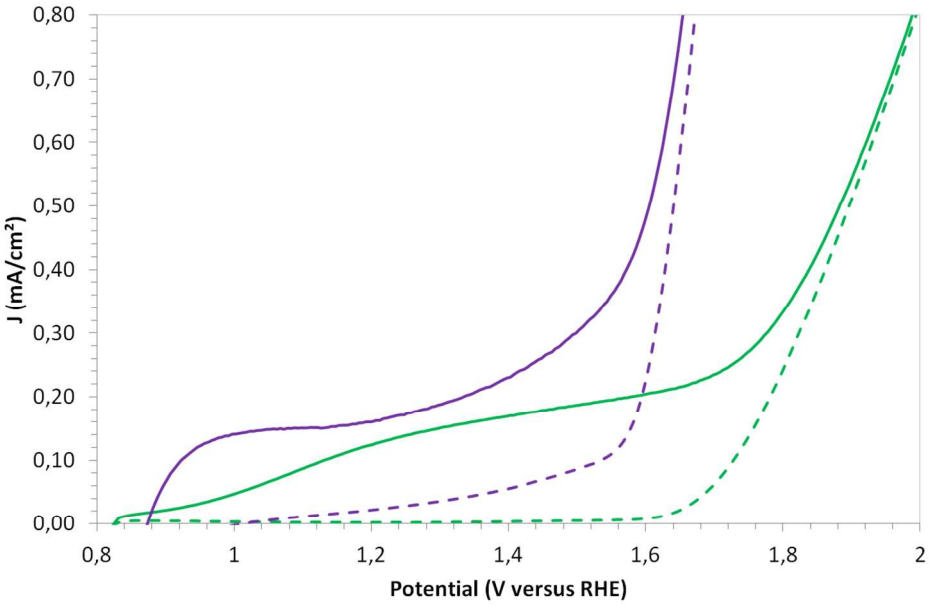

Figure 7. Modification of the surface chemistry by decorating the surface with Co−based catalyst. Current density *vs.* applied potential (*J*−*V*) plots in dark (dotted line) and under visible light illumination of mesoporous $Fe_{0.2}$−TiO_2 thin film with (purple) and without (green) a Co−Pi catalyst in contact with NaOH electrolyte.

It is commonly observed that heat treatment under reducing atmosphere leads to the reduction of Fe^{3+} to Fe^{2+}. This reducing treatment affects also the oxygen vacancies in the films and then the charge carrier density. Under these conditions, hole transport might be facilitated and as consequence, the photoelectrochemical response should be affected. Under this assumption, the photoelectrochemical properties of mesoporous $Fe_{0.2}$−TiO_2 films that were post heat−treated at

200°C and 300°C under 5% H_2 in Ar for 30 min were studied. Prior to electrochemical experiments, the structure and the microstructure of the reduced $Fe_{0.2}$−TiO_2 films were studied by X−ray diffraction and FE−SEM analyses. The treatment under H_2 does not affect the structure and the microstructure of the film (Figures S8 and S9). The current density vs. applied potential (J−V) under illumination is reported in Figure 8. The CV behavior is comparable to the one observed for mesoporous $Fe_{0.2}$-TiO_2 films heated at 500°C in air. At 1.2 V *vs.* RHE, visible light irradiation led to photocurrent density of 0.25 mA/cm^2. This current enhancement under light irradiation is attributed to the presence of Fe^{2+} that was also confirmed by ^{57}Fe Mössbauer spectroscopy. However, Fe^{2+} is unstable under the conditions of these tests and a gradual oxidation of Fe^{2+} into Fe^{3+} is observed that is confirmed by a decrease of the photocurrent with time (Fig. S10).

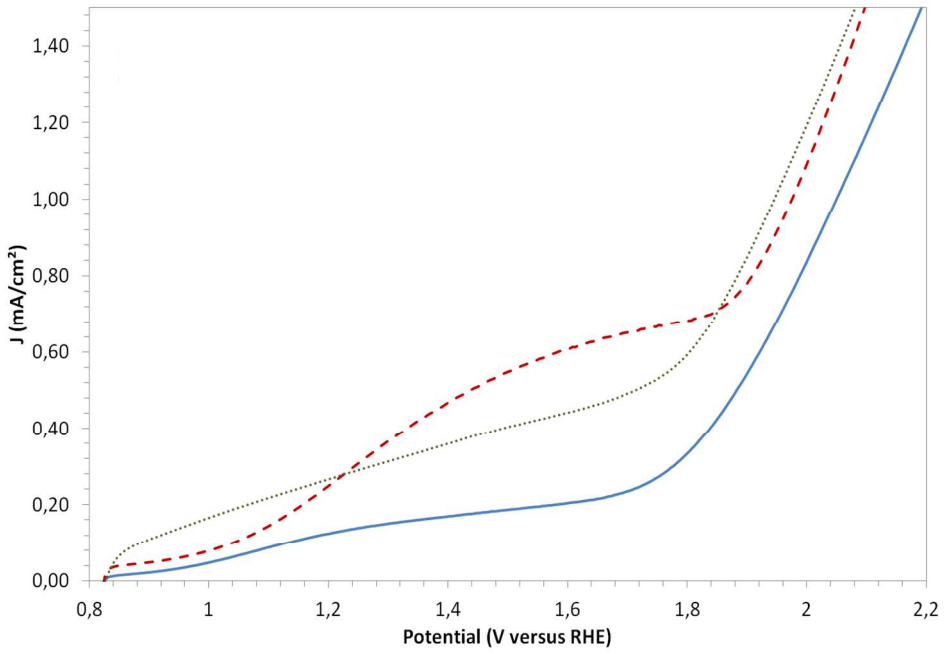

Figure 8. Modification of the oxidation state of Fe into Fe−TiO_2 films. Current density vs. applied potential (*J*−*V*) plots under illumination of mesoporous $Fe_{0,2}$-TiO_2 electrodes annealed at

500 °C under air (blue curve), post−heat−treated under 5%H_2 in Ar at 200°C for 30 min (dashed red curve), at 300°C for 30 min (dashed green curve).

The establishment of a photocurrent density as high as 0.25 mA/cm^2 with an onset potential of 0.8 V vs. RHE is quite remarkable if compared with values reported in the literature for related mesoporous Fe_2O_3 photoanodes [37]. Indeed, for Fe_2O_3 mesoporous films synthesized in the same conditions, after heat-treatment at 500°C, no photocurrent was obtained under visible light illumination. That nicely demonstrates the advantage of using nanoheterostructures composed of oxide with different structures and compositions where the hole can be stabilized at the solid/solid interface. As a consequence, the e^-/h^+ recombination in the bulk is tuned and in−fine high photo−currents can be achieved.

Conclusion

We have successfully employed a multi−layer template−directed sol−gel technique for the synthesis of mesoporous nanostructured Fe_x−TiO_2 films with tunable thickness and composition (x). These films are constituted of well−defined nanocrystallites, with small size and an interconnected network of pores. For high Fe content (x), the pore walls are constituted of various components such as Fe−doped anatase, pseudo−brookite and traces of hematite. These films, available at low cost and through a highly controllable process, display the qualities required for photoelectrochemical applications: optical transparency in the visible region, high specific surface area to reach high interface with the electrolyte and high densities of electro−active components, numerous solid/solid interface that stabilize hole and as consequence avoid the e^-/h recombination in the bulk. Experiments performed in electrolyte containing H_2O_2 indicate that the hole recombination occurs at the surface and may be suppressed trough the deposition of efficient electro-catalyst. As a proof of concept, “Co−based electro−catalyst” was

then successfully deposited at the surface of the electrode and cathodic photocurrents were established under visible light illumination. Films containing both Fe^{2+} and Fe^{3+} oxidation states exhibit higher photocurrent even though Fe^{2+} should be stabilized by doping the structure with another metallic cation for instance. A value of 0.15 mA/cm^2 at 1.23 V vs RHE was found for the Fe_x- TiO_2 film with x = 0.2. This work indicates that the use of nanoheterostructures in mesoporous films represents a promising design for the development of new architectures for the next technologies in artificial water splitting.

AUTHOR INFORMATION

Corresponding Author

*christel.laberty@upmc.fr;

Author Contributions

The manuscript was written through contributions of all authors. All authors have given approval to the final version of the manuscript. ‡These authors contributed equally. (match statement to author names with a symbol)

ACKNOWLEDGMENT

The authors thank Sandra Casale, from Service de Microscopie Electronique (Paris VI), for the HR-TEM observations and David Montero, from IMPC, for the SE-FEG images. We thank Christophe Méthivier, from the LRS for the XPS experiments. We thank Michel Fialin, from CAMPARIS, for microprobe measurements. We also thank Noémie Elgrishi from LCPB, Collège de France, for gas chromatography measurements.

REFERENCES

1. Lewis, N. S.; Nocera, D. G., Powering the planet: Chemical challenges in solar energy utilization. *Proceedings of the National Academy of Sciences* **2006,** *103* (43), 15729-15735.

2. Nocera, D. G., Personalized Energy: The Home as a Solar Power Station and Solar Gas Station. *ChemSusChem* **2009,** *2* (5), 387-390.
3. Sivula, K.; Le Formal, F.; Grätzel, M., Solar Water Splitting: Progress Using Hematite (α-Fe2O3) Photoelectrodes. *ChemSusChem* **2011,** *4* (4), 432-449.
4. Minggu, L. J.; Daud, W. R. W.; Kassim, M. B., An overview of photocells and photoreactors for photoelectrochemical water splitting. *International Journal of Hydrogen Energy* **2010,** *35* (11), 5233-5244.
5. Fujishima, A.; Honda, K., Electrochemical Photolysis of Water at a Semiconductor Electrode. *Nature* **1972,** *238* (5358), 37-38.
6. Gratzel, M., Photoelectrochemical cells. *Nature* **2001,** *414* (6861), 338-344.
7. Carp, O.; Huisman, C. L.; Reller, A., Photoinduced reactivity of titanium dioxide. *Progress in Solid State Chemistry* **2004,** *32* (1–2), 33-177.
8. Linsebigler, A. L.; Lu, G.; Yates, J. T., Photocatalysis on TiO2 Surfaces: Principles, Mechanisms, and Selected Results. *Chemical Reviews* **1995,** *95* (3), 735-758.
9. Choi, W.; Termin, A.; Hoffmann, M. R., The Role of Metal Ion Dopants in Quantum-Sized TiO2: Correlation between Photoreactivity and Charge Carrier Recombination Dynamics. *The Journal of Physical Chemistry* **1994,** *98* (51), 13669-13679.
10. Marusak, L. A.; Messier, R.; White, W. B., Optical absorption spectrum of hematite, αFe2O3 near IR to UV. *Journal of Physics and Chemistry of Solids* **1980,** *41* (9), 981-984.
11. Khan, M. A.; Woo, S. I.; Yang, O. B., Hydrothermally stabilized Fe(III) doped titania active under visible light for water splitting reaction. *International Journal of Hydrogen Energy* **2008,** *33* (20), 5345-5351.
12. Ranjit, K. T.; Viswanathan, B., Synthesis, characterization and photocatalytic properties of iron-doped TiO2 catalysts. *Journal of Photochemistry and Photobiology A: Chemistry* **1997,** *108* (1), 79-84.
13. Li, X.; Yue, P.-L.; Kutal, C., Synthesis and photocatalytic oxidation properties of iron doped titanium dioxide nanosemiconductor particles. *New Journal of Chemistry* **2003,** *27* (8), 1264-1269.
14. Dholam, R.; Patel, N.; Adami, M.; Miotello, A., Hydrogen production by photocatalytic water-splitting using Cr- or Fe-doped TiO2 composite thin films photocatalyst. *International Journal of Hydrogen Energy* **2009,** *34* (13), 5337-5346.
15. Mor, G. K.; Prakasam, H. E.; Varghese, O. K.; Shankar, K.; Grimes, C. A., Vertically Oriented Ti−Fe−O Nanotube Array Films: Toward a Useful Material Architecture for Solar Spectrum Water Photoelectrolysis. *Nano Letters* **2007,** *7* (8), 2356-2364.
16. Adán, C.; Bahamonde, A.; Fernández-García, M.; Martínez-Arias, A., Structure and activity of nanosized iron-doped anatase TiO2 catalysts for phenol photocatalytic degradation. *Applied Catalysis B: Environmental* **2007,** *72* (1–2), 11-17.
17. Kuang, S. Y.; Yang, L. X.; Luo, S. L.; Cai, Q. Y., Fabrication, characterization and photoelectrochemical properties of Fe2O3 modified TiO2 nanotube arrays. *Applied Surface Science* **2009,** *255* (16), 7385-7388.
18. Bickley, R. I.; Gonzalezcarreno, T.; Gonzalezelipe, A. R.; Munuera, G.; Palmisano, L., CHARACTERIZATION OF IRON TITANIUM-OXIDE PHOTOCATALYSTS .2. SURFACE STUDIES. *Journal of the Chemical Society-Faraday Transactions* **1994,** *90* (15), 2257-2264.
19. Kronawitter, C. X.; Vayssieres, L.; Shen, S. H.; Guo, L. J.; Wheeler, D. A.; Zhang, J. Z.; Antoun, B. R.; Mao, S. S., A perspective on solar-driven water splitting with all-oxide hetero-nanostructures. *Energy & Environmental Science* **2011,** *4* (10), 3889-3899.

20. Yu, J. G.; Yu, H. G.; Ao, C. H.; Lee, S. C.; Yu, J. C.; Ho, W. K., Preparation, characterization and photocatalytic activity of in situ Fe-doped TiO2 thin films. *Thin Solid Films* **2006,** *496* (2), 273-280.
21. Peng, L. L.; Xie, T. F.; Lu, Y. C.; Fan, H. M.; Wang, D. J., Synthesis, photoelectric properties and photocatalytic activity of the Fe2O3/TiO2 heterogeneous photocatalysts. *Physical Chemistry Chemical Physics* **2010,** *12* (28), 8033-8041.
22. Zhang, X. W.; Lei, L. C., Preparation of photocatalytic Fe2O3-TiO2 coatings in one step by metal organic chemical vapor deposition. *Applied Surface Science* **2008,** *254* (8), 2406-2412.
23. Young, K. M. H.; Klahr, B. M.; Zandi, O.; Hamann, T. W., Photocatalytic water oxidation with hematite electrodes. *Catalysis Science & Technology* **2013,** *3* (7), 1660-1671.
24. Zandi, O.; Klahr, B. M.; Hamann, T. W., Highly photoactive Ti-doped alpha-Fe2O3 thin film electrodes: resurrection of the dead layer. *Energy & Environmental Science* **2013,** *6* (2), 634-642.
25. Oh, H. J.; Noh, K. J.; Kim, B. R.; Kang, W.; Jung, S. C.; Kim, S. J., Fabrication of Fe2O3/TiO2 Photoanode for Improved Photoelectrochemical Water Splitting. *Japanese Journal of Applied Physics* **2013,** *52* (1).
26. Hamann, T. W., Splitting water with rust: hematite photoelectrochemistry. *Dalton Transactions* **2012,** *41* (26), 7830-7834.
27. Lindgren, T.; Wang, H. L.; Beermann, N.; Vayssieres, L.; Hagfeldt, A.; Lindquist, S. E., Aqueous photoelectrochemistry of hematite nanorod array. *Solar Energy Materials and Solar Cells* **2002,** *71* (2), 231-243.
28. Beermann, N.; Vayssieres, L.; Lindquist, S. E.; Hagfeldt, A., Photoelectrochemical studies of oriented nanorod thin films of hematite. *Journal of the Electrochemical Society* **2000,** *147* (7), 2456-2461.
29. Bjorksten, U.; Moser, J.; Gratzel, M., PHOTOELECTROCHEMICAL STUDIES ON NANOCRYSTALLINE HEMATITE FILMS. *Chemistry of Materials* **1994,** *6* (6), 858-863.
30. Qi, L. H.; Liu, Y. J.; Li, C. Y., Controlled synthesis of TiO2-B nanowires and nanoparticles for dye-sensitized solar cells. *Applied Surface Science* **2010,** *257* (5), 1660-1665.
31. Wen, X. G.; Wang, S. H.; Ding, Y.; Wang, Z. L.; Yang, S. H., Controlled growth of large-area, uniform, vertically aligned arrays of alpha-Fe2O3 nanobelts and nanowires. *Journal of Physical Chemistry B* **2005,** *109* (1), 215-220.
32. Mohapatra, S. K.; John, S. E.; Banerjee, S.; Misra, M., Water Photooxidation by Smooth and Ultrathin alpha-Fe2O3 Nanotube Arrays. *Chemistry of Materials* **2009,** *21* (14), 3048-3055.
33. Kay, A.; Cesar, I.; Gratzel, M., New benchmark for water photooxidation by nanostructured alpha-Fe2O3 films. *Journal of the American Chemical Society* **2006,** *128* (49), 15714-15721.
34. Maeda, K., Photocatalytic water splitting using semiconductor particles: History and recent developments. *Journal of Photochemistry and Photobiology C-Photochemistry Reviews* **2011,** *12* (4), 237-268.
35. Yu, J. C.; Wang, X. C.; Fu, X. Z., Pore-wall chemistry and photocatalytic activity of mesoporous titania molecular sieve films. *Chemistry of Materials* **2004,** *16* (8), 1523-1530.
36. Sakatani, Y.; Grosso, D.; Nicole, L.; Boissiere, C.; Soler-Illia, G.; Sanchez, C., Optimised photocatalytic activity of grid-like mesoporous TiO2 films: effect of crystallinity, pore size distribution, and pore accessibility. *Journal of Materials Chemistry* **2006,** *16* (1), 77-82.
37. Hamd, W.; Cobo, S.; Fize, J.; Baldinozzi, G.; Schwartz, W.; Reymermier, M.; Pereira, A.; Fontecave, M.; Artero, V.; Laberty-Robert, C.; Sanchez, C., Mesoporous alpha-Fe2O3 thin

films synthesized via the sol-gel process for light-driven water oxidation. *Physical Chemistry Chemical Physics* **2012,** *14* (38), 13224-13232.
38. Lancelle-Beltran, E.; Prene, P.; Boscher, C.; Belleville, P.; Buvat, P.; Lambert, S.; Guillet, F.; Boissiere, C.; Grosso, D.; Sanchez, C., Nanostructured hybrid solar cells based on self-assembled mesoporous titania thin films. *Chemistry of Materials* **2006,** *18* (26), 6152-6156.
39. Riha, S. C.; Klahr, B. M.; Tyo, E. C.; Seifert, S.; Vajda, S.; Pellin, M. J.; Hamann, T. W.; Martinson, A. B. F., Atomic Layer Deposition of a Submonolayer Catalyst for the Enhanced Photoelectrochemical Performance of Water Oxidation with Hematite. *Acs Nano* **2013,** *7* (3), 2396-2405.
40. Dotan, H.; Sivula, K.; Gratzel, M.; Rothschild, A.; Warren, S. C., Probing the photoelectrochemical properties of hematite (alpha-Fe2O3) electrodes using hydrogen peroxide as a hole scavenger. *Energy & Environmental Science* **2011,** *4* (3), 958-964.
41. Tilley, S. D.; Cornuz, M.; Sivula, K.; Gratzel, M., Light-Induced Water Splitting with Hematite: Improved Nanostructure and Iridium Oxide Catalysis. *Angewandte Chemie-International Edition* **2010,** *49* (36), 6405-6408.
42. Li, J. T.; Meng, F. K.; Suri, S.; Ding, W. Q.; Huang, F. Q.; Wu, N. Q., Photoelectrochemical performance enhanced by a nickel oxide-hematite p-n junction photoanode. *Chemical Communications* **2012,** *48* (66), 8213-8215.
43. Klahr, B.; Gimenez, S.; Fabregat-Santiago, F.; Bisquert, J.; Hamann, T. W., Photoelectrochemical and Impedance Spectroscopic Investigation of Water Oxidation with "Co-Pi"-Coated Hematite Electrodes. *Journal of the American Chemical Society* **2012,** *134* (40), 16693-16700.
44. Zhong, D. K.; Gamelin, D. R., Photoelectrochemical Water Oxidation by Cobalt Catalyst ("Co-Pi")/alpha-Fe2O3 Composite Photoanodes: Oxygen Evolution and Resolution of a Kinetic Bottleneck. *Journal of the American Chemical Society* **2010,** *132* (12), 4202-4207.
45. Meng, H. X.; Wang, B. B.; Liu, S.; Jiang, R. Y.; Long, H., Hydrothermal preparation, characterization and photocatalytic activity of TiO2/Fe-TiO2 composite catalysts. *Ceramics International* **2013,** *39* (5), 5785-5793.
46. Brinker, C. J.; Lu, Y. F.; Sellinger, A.; Fan, H. Y., Evaporation-induced self-assembly: Nanostructures made easy. *Advanced Materials* **1999,** *11* (7), 579-+.
47. Simeone, D.; Baldinozzi, G.; Gosset, D.; Zalczer, G.; Berar, J. F., Rietveld refinements performed on mesoporous ceria layers at grazing incidence. *Journal of Applied Crystallography* **2011,** *44*, 1205-1210.
48. Baldinozzi, G.; Muller, G.; Laberty-Robert, C.; Gosset, D.; Simeone, D.; Sanchez, C., Probing Properties, Stability, and Performances of Hierarchical Mesoporous Materials with Nanoscale Interfaces. *Journal of Physical Chemistry C* **2012,** *116* (14), 7658-7663.
49. Bérar, J. F.; Baldinozzi, G., Xnd code: from x-ray laboratory data to incommensurately modulated phases. Rietveld modelling of complex materials. *IUCr CPD Newsletter* **1998,** *20*, 3-5.
50. Guo, W. Q.; Malus, S.; Ryan, D. H.; Altounian, Z., Crystal structure and cation distributions in the FeTi2O5-Fe2TiO5 solid solution series. *Journal of Physics-Condensed Matter* **1999,** *11* (33), 6337-6346.
51. Bhargava, G.; Gouzman, I.; Chun, C. M.; Ramanarayanan, T. A.; Bernasek, S. L., Characterization of the "native" surface thin film on pure polycrystalline iron: A high resolution XPS and TEM study. *Applied Surface Science* **2007,** *253* (9), 4322-4329.

52. Joseph, C. M.; Binu, P. R.; Shreekrishnakumar, K.; Menon, C. S., Preparation and physical properties of CuPc substituted sodium borate glass matrix. *Materials Letters* **2002,** *53* (4-5), 326-328.
53. Tyagi, P.; Vedeshwar, A. G., Grain size dependent optical band gap of CdI2 films. *Bulletin of Materials Science* **2001,** *24* (3), 297-300.
54. Miao, L.; Jin, P.; Kaneko, K.; Terai, A.; Nabatova-Gabain, N.; Tanemura, S., Preparation and characterization of polycrystalline anatase and rutile TiO2 thin films by rf magnetron sputtering. *Applied Surface Science* **2003,** *212*, 255-263.
55. Ni, M.; Leung, M. K. H.; Leung, D. Y. C.; Sumathy, K., A review and recent developments in photocatalytic water-splitting using TiO2 for hydrogen production. *Renewable & Sustainable Energy Reviews* **2007,** *11* (3), 401-425.
56. Ginley, D. S.; Butler, M. A., PHOTOELECTROLYSIS OF WATER USING IRON TITANATE ANODES. *Journal of Applied Physics* **1977,** *48* (5), 2019-2021.
57. Tatlıdil, İ.; Bacaksız, E.; Buruk, C. K.; Breen, C.; Sökmen, M., A short literature survey on iron and cobalt ion doped TiO2 thin films and photocatalytic activity of these films against fungi. *Journal of Alloys and Compounds* **2012,** *517* (0), 80-86.
58. Peter, L. M., Dynamic aspects of semiconductor photoelectrochemistry. *Chemical Reviews* **1990,** *90* (5), 753-769.
59. Cummings, C. Y.; Marken, F.; Peter, L. M.; Tahir, A. A.; Wijayantha, K. G. U., Kinetics and mechanism of light-driven oxygen evolution at thin film alpha-Fe2O3 electrodes. *Chemical Communications* **2012,** *48* (14), 2027-2029.